PNAS RESEARCH ARTICLE | MICROBIOLOGY OPEN ACCESS

Crystal structures of YeiE from *Cronobacter sakazakii* and the role of sulfite tolerance in gram-negative bacteria

Seokho Hong[a,b,1], Jinshil Kim[a,b,1], Eunshin Cho[a,b], Soohui Na[a,b], Yeon-Ji Yoo[c], You-Hee Cho[c], Sangryeol Ryu[a,b,2], and Nam-Chul Ha[a,b,2]

Edited by Gisela Storz, National Institute of Child Health and Human Development, Bethesda, MD; received September 30, 2021; accepted February 7, 2022

Cronobacter sakazakii **is an emerging gram-negative pathogenic bacterium that causes meningitis, bacteremia, and necrotizing enterocolitis in infants and has a high mortality rate. The YeiE homolog (gpESA_01081) was identified as a global virulence regulator of bacterial pathogenesis in *C. sakazakii*. YeiE is a LysR-type transcriptional regulator (LTTR) composed of a DNA binding domain and a regulatory domain to recognize the unknown ligand. To reveal the molecular mechanism and function of YeiE, we determined the crystal structure of the regulatory domain of YeiE. A sulfite ion was bound at the putative ligand-binding site, and subsequent studies revealed that the sulfite is the physiological ligand for YeiE. Structural comparisons to its sulfite-free structure further showed the sulfite-dependent conformational change of YeiE. The essential role of YeiE in defending against toxicity from sulfite during the growth of *C. sakazakii* and *Escherichia coli* was examined. Furthermore, the target genes and functional roles of YeiE in H_2S production and survival capability from neutrophils were investigated. Our findings provide insights into the sophisticated behaviors of pathogenic gram-negative bacteria in response to sulfite from the environment and host.**

YeiE | LysR-type transcriptional regulator | sulfite | hydrogen sulfide | sulfite reductase

Cronobacter sakazakii (formerly known as *Enterobacter sakazakii*) is an emerging gram-negative pathogen that causes life-threatening symptoms. This bacterium can cause meningitis, bacteremia, and necrotizing enterocolitis in infants, with high mortality rates (1–7). *C. sakazakii* has many virulence characteristics, such as biofilm formation to resist environmental stresses (8, 9). This bacterium can invade host cells and shows continued survival within macrophages (10). Along with macrophages, neutrophils are recruited to the mucous membrane lamina propria and contribute to the initial clearance of *C. sakazakii* infection (11). *C. sakazakii* has been found in various foods, including dairy products, meats, drinking water, and dried fish products (1, 12–16). Powdered infant formula is one of the primary sources of bacterial contamination and infections, representing a critical issue for infant health (6).

For the pathogenesis of invading bacteria, the bacterial transcription factors OxyR, HypT, and RclR are specific sensors of the individual reactive oxygen species (ROS) generated by the host immune system, inducing the appropriate genes scavenging each ROS stress (17–20). In particular, OxyR belongs to a tetrameric LysR-type transcriptional regulator (LTTR) that recognizes hydrogen peroxide (H_2O_2) and induces the catalase-peroxidase KatG (21). LTTRs consist of an N-terminal DNA binding domain (DBD) and a C-terminal regulatory domain (RD) that contains the ligand-binding site between the subdomains RD-I and RD-II (22). The typical LTTRs form an asymmetric (21) or symmetric (23, 24) tetrameric arrangement between the two dimeric interactions of DBD to DBD and RD to RD. The binding of the cognate ligand to the RD induces a conformational change of the RD that is typically characterized by the closing motion between the subdomains RD-I and RD-II in the RD. The conformational change in the RDs leads to the relative movements of the DBDs in the tetramer, which changes the DNA binding ability or the binding sequences of the LTTRs.

In a previous study, the LTTR homolog, gpESA_01081, was a global regulator of virulence in *C. sakazakii* (25). This LTTR protein plays a critical role in the pathogenesis-associated phenotypes of *C. sakazakii*, such as human intestinal cell invasion, biofilm formation, oxidative stress resistance, and induction of proinflammatory cytokines (25). However, the mechanism underlying the ability of LTTR to contribute to the pathogenicity of *C. sakazakii* is largely unknown at the molecular level. Herein, we determined the crystal structures of the LTTR of *C. sakazakii*, which unexpectedly contained a sulfite ion at the canonic ligand-binding site. The bound sulfite has molecular implications for the roles of the LTTR YeiE in sensing and tolerating sulfite in bacteria.

Significance

YeiE has been identified as a master virulence factor of *Cronobacter sakazakii*. In this study, we determined the crystal structures of the regulatory domain of YeiE in complex with its physiological ligand sulfite ion (SO_3^{2-}). The structure provides the basis for the molecular mechanisms for sulfite sensing and the ligand-dependent conformational changes of the regulatory domain. The genes under the control of YeiE in response to sulfite were investigated to reveal the functional roles of YeiE in the sulfite tolerance of the bacteria. We propose the molecular mechanism underlying the ability of gram-negative pathogens to defend against the innate immune response involving sulfite, thus providing a strategy to control the pathogenesis of bacteria.

Author contributions: S.H., S.R., and N.-C.H. designed research; S.H., J.K., E.C., S.N., Y.-J.Y., and Y.-H.C. performed research; S.H., J.K., E.C., Y.-H.C., S.R., and N.-C.H. analyzed data; and S.H., J.K., and N.-C.H. wrote the paper.

The authors declare no competing interest.

This article is a PNAS Direct Submission.

[1]S.H. and J.K. contributed equally to this work.

[2]To whom correspondence may be addressed. Email: sangryu@snu.ac.kr or hanc210@snu.ac.kr.

This article contains supporting information online at http://www.pnas.org/lookup/suppl/doi:10.1073/pnas.2118002119/-/DCSupplemental.

Published March 10, 2022.

Results

Determination of the Crystal Structure of CsYeiE RD and Its Dimeric Assembly. The homologs of *C. sakazakii* gpESA_01081 [called the LTTR homolog (25)] have been found in most pathogenic gram-negative bacteria, such as *Escherichia coli*, *Salmonella enterica*, and *Pseudomonas aeruginosa* (*SI Appendix*, Fig. S1*A*). In *E. coli*, the homolog was named YeiE, and it functions as a transcriptional activator of *lysP* to increase lysine uptake and maintain iron homeostasis under iron-limited conditions (26, 27). Deletion of *yeiE* in *Salmonella* resulted in a significant defect in swimming motility, gut colonization, and attenuated neutrophil respiratory burst by the bacteria (28, 29). We named the *C. sakazakii* gpESA_01081 YeiE (CsYeiE) in this study.

As an initial attempt to gain insights into the molecular mechanism by which CsYeiE functions in *C. sakazakii*, we determined the crystal structure of the RD of CsYeiE (residues 85 to 288) at a 2.0-Å resolution by the molecular replacement method. The model for the molecular replacement was generated by the artificial intelligence algorithm program T-fold (Tencent AI Lab) (*SI Appendix*, Fig. S2). The overall structure of CsYeiE RD exhibited the typical features of the LTTR RD (21, 23, 30–33) (*SI Appendix*, Fig. S1*B*). Two protomers of CsYeiE RD were assembled in a homodimer interacting between RD-I from one protomer and RD-II from the other protomer within the asymmetric unit (Fig. 1*A*). The angle between each protomer is ∼60° along an axis perpendicular to the twofold axis, similar to that of the LTTR QuiR RD dimer of *Listeria monocytogenes* in the ligand-induced active state (34) (Fig. 1 *B* and *C*). This structural similarity suggests that the crystal structure of the CsYeiE RD dimer represents the ligand-binding state.

YeiE Is a Sulfite-Specific LTTR. CsYeiE has canonic ligand-binding sites at the RD-I and RD-II interfaces, similar to many LTTRs. Notably, we found additional electron density maps displaying a trigonal pyramid in the ligand-binding site (*SI Appendix*, Fig. S3). Since the surface representation of CsYeiE RD revealed that the molecule is in a small cavity accessible from the solvent, the molecule seems to be the ligand for YeiE (Fig. 2*A*). The ligand-binding sites were lined with Ser96, Ser97, Asn126, Ser127, Glu145, Arg191, Ser195, and Thr197 residues (Fig. 2*A*), which are mostly conserved among the YeiE homologs.

To gain clues to identify the bound molecule, we searched proteins with similar ligand-binding sites using the BLAST program, focusing on the lining residues in the ligand-binding site. We noted the LTTR CysL of the top solutions in the multiple sequence alignments, only found in gram-positive bacteria. Although the structure of CysL is not available, CysL is required to grow in a sulfate- or sulfite-containing medium by inducing the sulfite reductase complex CysJI for cysteine biosynthesis in the presence of sulfate or sulfite (35). Since sulfite ions exhibit a trigonal pyramid geometry, we added a sulfite ion to the structural model of CsYeiE RD and then further refined the structure. The sulfite was nicely fitted to the electron density map in the ligand-binding site (*SI Appendix*, Fig. S3*D*).

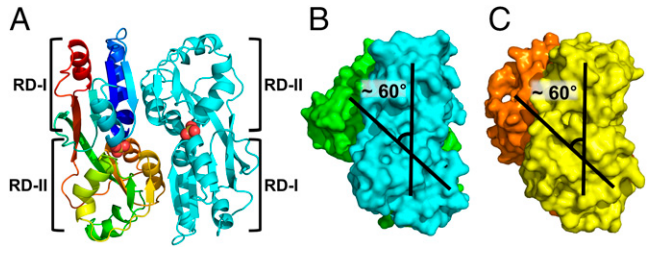

Fig. 1. Dimeric arrangement of CsYeiE RD. (*A*) Dimeric structure of sulfite-bound CsYeiE RD. Chain A is in cyan, and chain B presents the colors of the rainbow from the N terminus (blue) to C terminus (red). RD-I and RD-II are indicated with brackets. The sulfite ions in the binding site are shown as spheres. (*B*) Side view of the sulfite-bound CsYeiE RD dimer in *A*. The dimeric angle (∼60°) between chain A (cyan) and chain B (green) of the CsYeiE RD dimer is shown with the axes. (*C*) Structural comparison of the dimer of *L. monocytogenes* QuiR RD in complex with an effector (shikimate) [Protein Data Bank: 5TED (34)] with the CsYeiE RD dimer in *B* (rmsd = 2.324 Å between 295 Cα atoms). The dimeric angle (∼60°) between two protomers of the *L. monocytogenes* QuiR RD dimer is shown with axes.

We measured the binding affinity of sulfite to CsYeiE RD using isothermal titration calorimetry (ITC). Nitrate ions (NO_3^-) with a trigonal planar geometry and sulfate ions (SO_4^{2-}) with tetrahedral geometry were also tested. The ITC results showed that CsYeiE RD has a binding affinity to sulfite (dissociation constant K_D = 1.38 μM) (Fig. 2*C*) but not to NO_3^- or SO_4^{2-} (*SI Appendix*, Fig. S4 *A* and *B*). Although the crystal structure suggested a stoichiometry of 1 with the bound sulfite ion, the measured stoichiometry was ∼0.5, which would be accounted for by the inactive or partially denatured proteins contained in the sample. Thus, our results demonstrate that YeiE is a sulfite-specific LTTR by distinguishing it from structurally similar compounds.

Glu145 of YeiE Is Responsible for Distinguishing Sulfite from Sulfate. In the crystal structure, the negatively charged oxygen atoms in the sulfite ion form an ionic bond with Arg191. The backbone NH groups and the side-chain hydroxyl groups of the lining residues form an extensive hydrogen bond network with the oxygen atoms in the sulfite ion (Fig. 2*B*). Notably, the sulfur atom of the sulfite ion is near the negatively charged side chain of Glu145 inside the YeiE structure, which is the only negatively charged residue in the ligand-binding pocket.

To dissect the role of Glu145, we determined the crystal structure of the mutant CsYeiE RD protein substituted with the serine residue with a smaller side chain in the presence of 10 mM sodium sulfate (Na_2SO_4) at a 2.05-Å resolution (*SI Appendix*, Fig. S5*A*). The CsYeiE RD E145S mutant contained SO_4^{2-} in place of the sulfite ion (Fig. 2*D* and *SI Appendix*, Fig. S6). In particular, the fourth oxygen atom of SO_4^{2-} occupied the expanded cavity by mutation without electrostatic repulsion. These results suggested that Glu145 provides selectivity to sulfite over sulfate based on the complementary space and charge in the ligand-binding pocket. The corresponding glutamate residue in CysL of gram-positive bacteria (*SI Appendix*, Fig. S7) also suggested that CysL is a sulfite-specific LTTR sharing structural organization with YeiE.

Structural Changes of CsYeiE RD by Sulfite Binding. To investigate the structural change by sulfite binding in YeiE, we determined the crystal structure of ligand-free CsYeiE RD using an extensively dialyzed protein sample in a different space group at a 1.95-Å resolution (*SI Appendix*, Fig. S5*B*). RD-II was more identical than RD-I in the structural superposition between the individual subdomains (rmsd values of 0.835 Å between 88 Cα atoms for RD-I and 0.373 Å between 83 Cα atoms for RD-II). The relative orientation between RD-I and RD-II within a protomer differed by ∼15° by structural superposition using RD-II as a reference, thus showing that RD-I moves closer to RD-II by sulfite binding (Fig. 3*A*). The structural comparison showed a closing motion by sulfite binding within the RD protomers, resulting in a rotational movement of the protomers in the dimeric assembly. The angle between one protomer and the

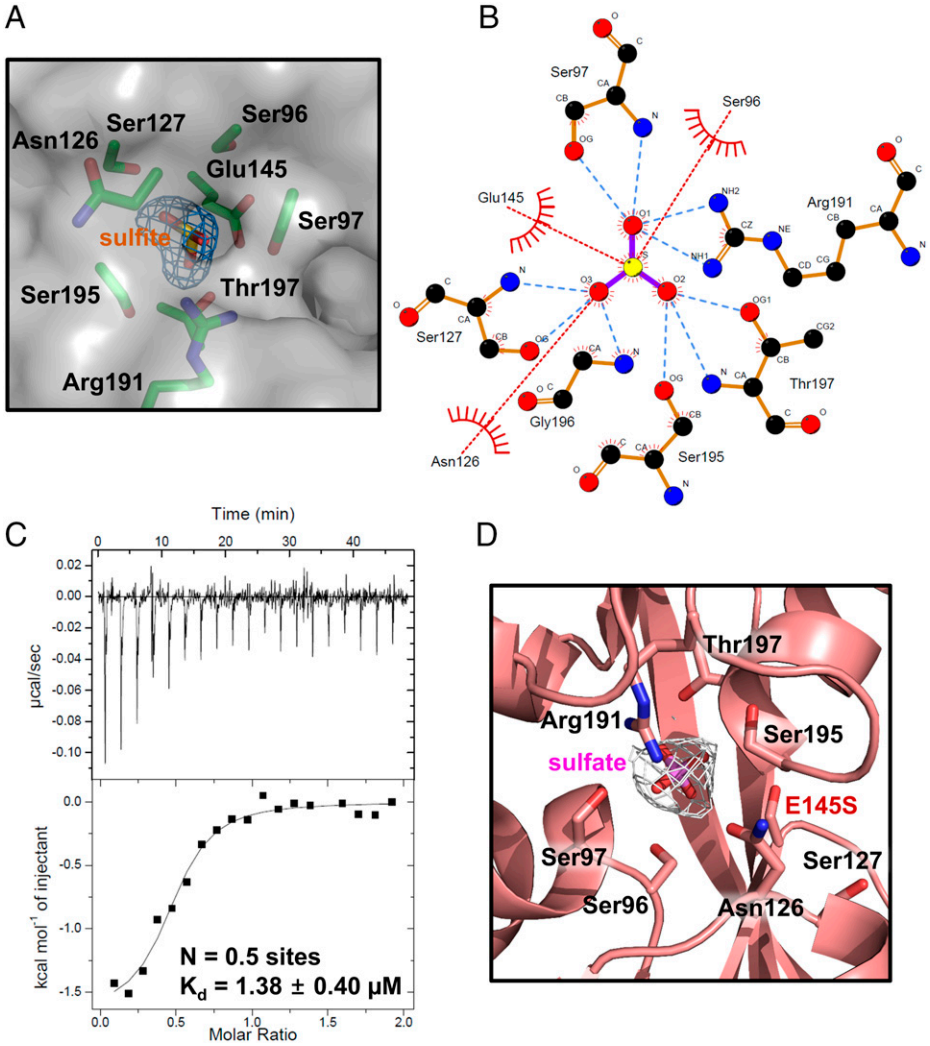

Fig. 2. Sulfite-binding site of CsYeiE. (*A*) Bound sulfite ion in the CsYeiE RD. The amino acids (green) surrounding the sulfite in the ligand-binding site of sulfite-bound CsYeiE RD are shown as a stick model. The protein surface is represented by transparent gray. The electron density map of sulfite is shown as blue mesh and contoured at 1.0 σ. (*B*) Schematic diagram of the interactions between sulfite ion and CsYeiE RD. The blue dotted lines represent hydrogen bonds, and the red dotted lines represent hydrophobic interactions. The residue and atom names are labeled at the side for each subject. The diagram was generated by LigPlot+ (52). (*C*) ITC graph for the titration of sulfite to CsYeiE RD. The ligand injection profile (raw data; *Top*) and the calculated heat/enthalpy change for each ligand injection (*Bottom*) are shown in the graph. The stoichiometry value (N) and K_D of CsYeiE RD with sulfite were calculated as 0.5 sites and 1.38 µM, respectively. (*D*) Bound SO_4^{2-} in the CsYeiE RD E145S. The sulfate-bound CsYeiE RD E145S is colored salmon, and the residues surrounding the sulfate are shown as a stick model. The SO_4^{2-} in CsYeiE RD E145S is colored pink and shown as a stick model. The electron density map of sulfate is shown as gray mesh and contoured at 1.0 σ.

other protomer of the sulfite-bound CsYeiE RD dimer is decreased by ∼7° compared to the ligand-free CsYeiE RD dimer structure (Fig. 3*B*).

In the sulfite-binding cavity of CsYeiE RD, the residues in RD-I of sulfite-bound CsYeiE RD were closer to RD-II than the corresponding residues in RD-I of ligand-free CsYeiE RD (Fig. 3*C*). In the ligand-free structure of CsYeiE RD, three water molecules (w1, w2, and w3 in Fig. 3 *D*, *Bottom*) were widely spread in the intersubdomain cavity, sharing the interacting residues with sulfite ion (Fig. 3 *D*, *Top*). However, since the distances between the water molecules are longer than the length between the S-O bond of sulfite ion, the interdomain cavity of the sulfite-free structure is more relaxed than that of the sulfite-bound structure, which explains the sulfite-dependent closing motion within the RD. Many LTTR structures have shown that the movement within RD in the full-length (FL) tetramer is transmitted to the relative motion between DBDs (21–23). Thus, the sulfite-dependent closing motion in the CsYeiE RD would regulate the transcriptional activity similar to many LTTRs. In addition, sulfite-induced structural stabilization was observed by the thermal shift assay (*SI Appendix*, Fig. S4*C*).

YeiE Is Required for the Growth of Gram-Negative Bacteria in Sulfite-Containing Media. To investigate the function of YeiE in *C. sakazakii*, we generated a *yeiE*-deleted (Δ*yeiE*) strain and a complemented strain (Δ*yeiE*+pYeiE) in the ATCC 29544 wild-type (WT) strain background. The bacterial strains were cultured in the sulfate-deficient M9 minimal media with various sodium sulfite (Na_2SO_3) concentrations (Fig. 4*A* and *SI Appendix*, Fig. S8*A*). The growth of all bacterial strains was restricted in the sulfate-deficient M9 medium (Fig. 4*A*, 0 mM). When Na_2SO_3 was supplemented at a concentration over 0.1 mM to the medium, the WT strain grew normally (Fig. 4*A*, WT, 0.1 to 1 mM). However, the growth of the Δ*yeiE* strain was retarded in the sulfate-deficient medium containing 0.1 mM sulfite, and the Δ*yeiE* strain lost viability in the presence of over 0.5 mM Na_2SO_3 (Fig. 4*A*, Δ*yeiE*, 0.5 mM).

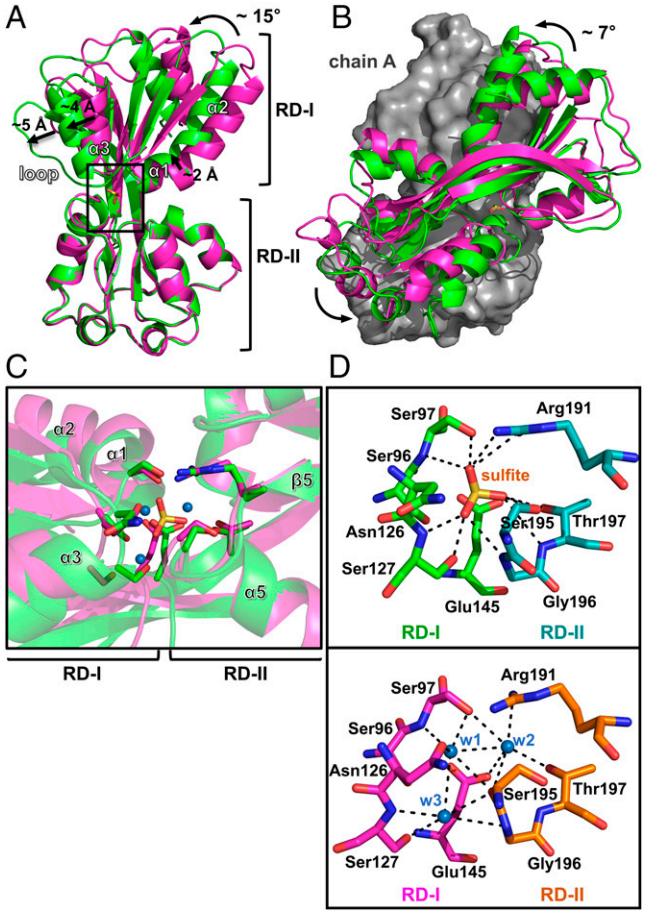

Fig. 3. Conformational changes of CsYeiE RD upon sulfite binding. (*A*) Structural superposition between RD-II in chain B of sulfite-bound CsYeiE RD (green) and RD-II in chain B of ligand-free CsYeiE RD (magenta) (rmsd = 0.373 Å between 83 Cα atoms). The rotation angle (~15°) between RD-I of sulfite-bound CsYeiE RD and RD-I of ligand-free CsYeiE RD and the length of the movements of the α-helices in RD-I are shown as arrows with each value. (*B*) Structural superposition between chain A of the sulfite-bound CsYeiE RD dimer and chain A of the ligand-free CsYeiE RD dimer (rmsd = 0.835 Å between 169 Cα atoms). The deviated angle (~7°) between chain B in the sulfite-bound CsYeiE RD dimer (green) and chain B in the ligand-free CsYeiE RD dimer (magenta) is shown as arrows with a value. Each chain A in both dimers is colored gray, and chain B of the sulfite-bound dimer and chain B of the ligand-free dimer are colored green and magenta, respectively. (*C*) A close-up view of the *Inset* in *A*. The residues surrounding the sulfite are shown as a stick model, and structures of CsYeiE RD are shown as a cartoon model. The α-helices, β-strand, RD-I, and RD-II of CsYeiE RD are indicated. (*D*) Critical residues in *C* are shown separately with observations from the same direction and same scale. *Top*: Sulfite-bound CsYeiE RD, green (RD-I) and light blue (RD-II). *Bottom*: Ligand-free CsYeiE RD, magenta (RD-I) and orange (RD-II). The sulfite in the sulfite-bound CsYeiE RD is shown as a yellow stick (*Top*), and the water molecules (w1, w2, and w3) in the ligand-free CsYeiE RD are shown as blue spheres (*Bottom*). The interactions between residues and sulfite or water molecules are represented with dotted lines.

When the *yeiE* gene was introduced into the Δ*yeiE* strain, the growth of the bacteria was recovered, albeit at slower growth rates (Fig. 4*A*, Δ*yeiE*+pYeiE, 0.1 to 1 mM). Our results indicate that YeiE is required for utilizing sulfite as the sulfur source for the growth of *C. sakazakii* and *C. sakazakii* could not achieve normal growth in the presence of over 0.5 mM sulfite without YeiE.

We next performed a similar experiment in Luria-Bertani (LB) medium containing a sufficient sulfur source to determine the role of YeiE in a general growth environment. The Δ*yeiE* strain of *C. sakazakii* showed growth defects when the LB media was supplemented with over 1 mM sulfite (Fig. 4*B*, Δ*yeiE*, 1 to 5 mM), indicating that sulfite is toxic to the growth of bacteria.

To address the conserved role of YeiE in other gram-negative bacteria, we performed similar experiments using the model bacteria *E. coli*. The MG1655 strain of *E. coli* (*E. coli* WT) and complemented strain of *E. coli* (*E. coli* Δ*yeiE*+pYeiE) grew at over 1 mM sulfite as the sulfur source and exhibited resistance to sulfite (*SI Appendix*, Fig. S8*B*). In contrast, *E. coli* Δ*yeiE* could not survive in the presence of high sulfite, as observed in *C. sakazakii* (*SI Appendix*, Fig. S8*B*). Thus, our findings suggest that YeiE exerts a crucial role in sensing and defending against sulfite stress during the growth of gram-negative bacteria.

YeiE Induces Sulfite Reductase to Convert Sulfite to H_2S. Bacteria have only a sulfite reduction pathway to metabolize sulfite, and the sulfite reductase complex CysJI in the pathway converts sulfite to hydrogen sulfide (H_2S). To examine the role of YeiE in sulfite reduction, we measured the amount of H_2S production in the WT, Δ*yeiE*, and complemented strains of *C. sakazakii*. In the presence of over 0.2 mM sulfite, H_2S production was evident in both the WT and the complemented strains (Fig. 4*C*). However, H_2S production was decreased in the Δ*yeiE* strain of *C. sakazakii* (Fig. 4*C*). Moreover, YeiE-dependent H_2S production was observed to a lesser extent in *E. coli* as well (*SI Appendix*, Fig. S9). Thus, our findings substantiated the role of YeiE in sulfite reduction in gram-negative bacteria.

Next, we were promoted to investigate other genes in *C. sakazakii* presumably responsible for bacterial H_2S production. The sulfite reductase CysJI complex synthesizes H_2S from sulfite, while CBS, CSE, 3MST, and AspC produce H_2S from cysteine in the cysteine metabolism (35–37). The transcriptional levels of *cysJ* and *cysI* were significantly increased in response to sulfite in the WT strain (Fig. 4*D*). However, the *cbs*, *cse*, *3MST*, and *aspC* genes were not induced by sulfite (*SI Appendix*, Fig. S10), indicating that YeiE is not involved in the cysteine metabolism. These observations indicate that YeiE decreases sulfite toxicity through the sulfite reductase CysJI complex by producing H_2S from sulfite in gram-negative bacteria.

We further investigated the role of CysJI in sulfite sensitivity concerning YeiE. The *cysJI*-deleted (Δ*cysJI*) strain of *C. sakazakii* showed less H_2S generation than the WT strain in the LB media (Fig. 5*A*). Consistently, the Δ*cysJI* strain showed a significant growth defect when sulfite was treated in the M9 medium supplemented with cysteine (Fig. 5*B*). Our results suggested that CysJI is the major contributor to bacterial growth in the presence of sulfite by converting the sulfite to gaseous H_2S, freely diffusible to the external medium.

We also carried out the electrophoretic mobility shift assay (EMSA) on the promoter region of the *cysJI* operon with the FL CsYeiE protein both in the presence and in the absence of sulfite (Fig. 5*C*). The CsYeiE protein was bound to the *cysJI* promoter region regardless of sulfite (Fig. 5*C*). These results demonstrated that YeiE transcriptionally activates the sulfite reductase *cysJI*. They further suggested that the sulfite-bound and sulfite-free forms of CsYeiE show a different binding mode on their target DNA sites, as observed in many LTTRs (21, 23).

YeiE Is Essential for Survival Response against Neutrophils. Given that YeiE is known as the global virulence regulator of *C. sakazakii*, we attempted to link the role of YeiE in the tolerance to the host immune system. Since neutrophils in the host immune system produce and secrete sulfite in response to

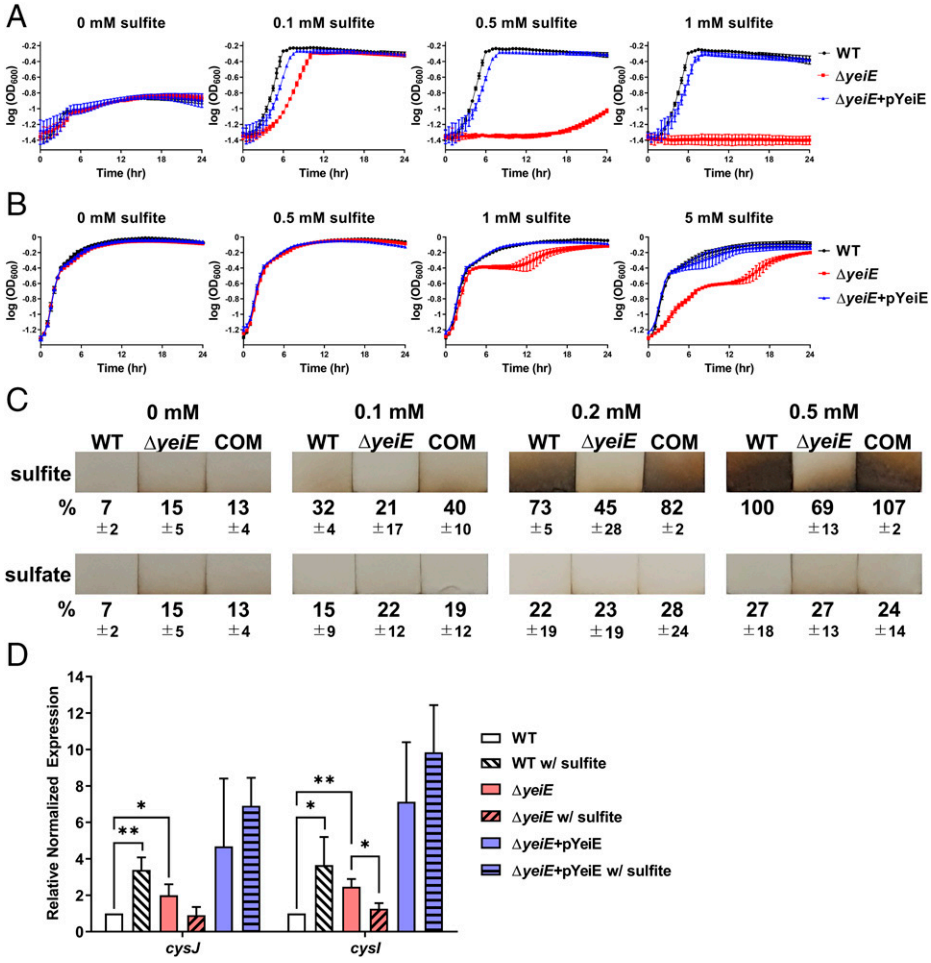

Fig. 4. Functional role of YeiE in defending against sulfite. (*A*) Growth curves of the WT strain, Δ*yeiE* strain, and complemented strain (Δ*yeiE*+pYeiE) of *C. sakazakii* in sulfate-deficient M9 media with Na_2SO_3 were measured by OD_{600}. The mean and SD values were calculated from three replicate experiments. (*B*) Growth curves of the WT strain, Δ*yeiE* strain, and Δ*yeiE*+pYeiE of *C. sakazakii* in LB media with Na_2SO_3 were measured by OD_{600}. The mean and SD values were calculated from three replicate experiments. (*C*) Amount of H_2S production of the WT strain, Δ*yeiE* strain, and complemented strain (COM) of *C. sakazakii* in liquid LB media was measured. The brown-stained paper strips show a result of the reaction with gaseous H_2S exiting in the liquid bacterial cultures. The percentages indicate the average level of H_2S production for each strain relative to the result of WT supplemented with 0.5 mM sulfite. The plus-minus sign represents SD values from three replicate experiments. (*D*) Target genes regulated in the WT strain, Δ*yeiE* strain, and *yeiE*+pYeiE of *C. sakazakii* upon exposure to sulfite (w/ sulfite) were confirmed by quantitative real-time PCR (qRT-PCR). Each column represents the transcript level (relative normalized expression) of genes. Error bars represent SD values calculated from three replicate experiments ($n = 3$), and the *P* value was calculated with an unpaired *t* test using GraphPad Prism 8.0 software. **P* < 0.05; ***P* < 0.005. Genes: sulfite reductase alpha-subunit *cysJ* and sulfite reductase beta-subunit *cysI*..

lipopolysaccharide (38), we examined the role of YeiE in the survival response against host neutrophils. In the neutrophil extracellular killing assay with freshly isolated bovine neutrophils, *yeiE* deletion in *C. sakazakii* dramatically reduced the viability of the bacteria after 30 min of exposure to neutrophils (Fig. 6*A*). When the bacteria were incubated for 1 h with neutrophils, the Δ*yeiE* strain showed only one-third of the survival rate compared to the WT strain (Fig. 6*A*). Thus, our results indicate that YeiE is a vital virulence factor in *C. sakazakii* in response to neutrophils, which may be related to YeiE-dependent bacterial resistance to the stress of sulfite.

Discussion

Many fungi secrete sulfite, along with antibiotics, to combat bacteria in the environment (39, 40). Humans have widely used sulfite salt as bleaching, antimicrobial, and reducing agents and an oxygen scavenger (41). The host innate immune system also employs sulfite, together with ROS, to efficiently kill invading bacteria. Our study revealed the structures and functions of YeiE as a transcription regulator that is responsive to sulfite, thus intervening in the gene expression pattern of the bacteria. We found that YeiE mediates the rapid decrease in sulfite by expressing sulfite reductase CysJI (Fig. 6*B*). YeiE also contributed to bacterial survival from neutrophils secreting sulfite.

Several pathogenic bacteria endogenously generate H_2S to protect the bacteria from antibiotics and oxidative stress (36, 37, 42). After exposure to sulfite, the elevated expression of sulfite reductase CysJI in *C. sakazakii* would consume sulfite and produce H_2S with bacterial survival in the sulfite-rich environments. We found that the production of H_2S was substantially increased by sulfite treatment only in the presence of YeiE (Fig. 4*C*). Since bacterial H_2S production was implicated in the tolerance to antibiotics and ROS (36, 37, 42), our finding of sulfite-dependent H_2S production would provide clues to reveal the sophisticated bacterial resistance mechanism against antibiotics and ROS stress from fungi and in the human body. Further study is required to provide additional insights into the underlying molecular mechanisms.

This study presented CysJI as the primary contributor to the YeiE-dependent sulfite resistance of the bacteria. However, the deletion of *cysJI* in *C. sakazakii* (Fig. 5*B*, over 5 mM) showed

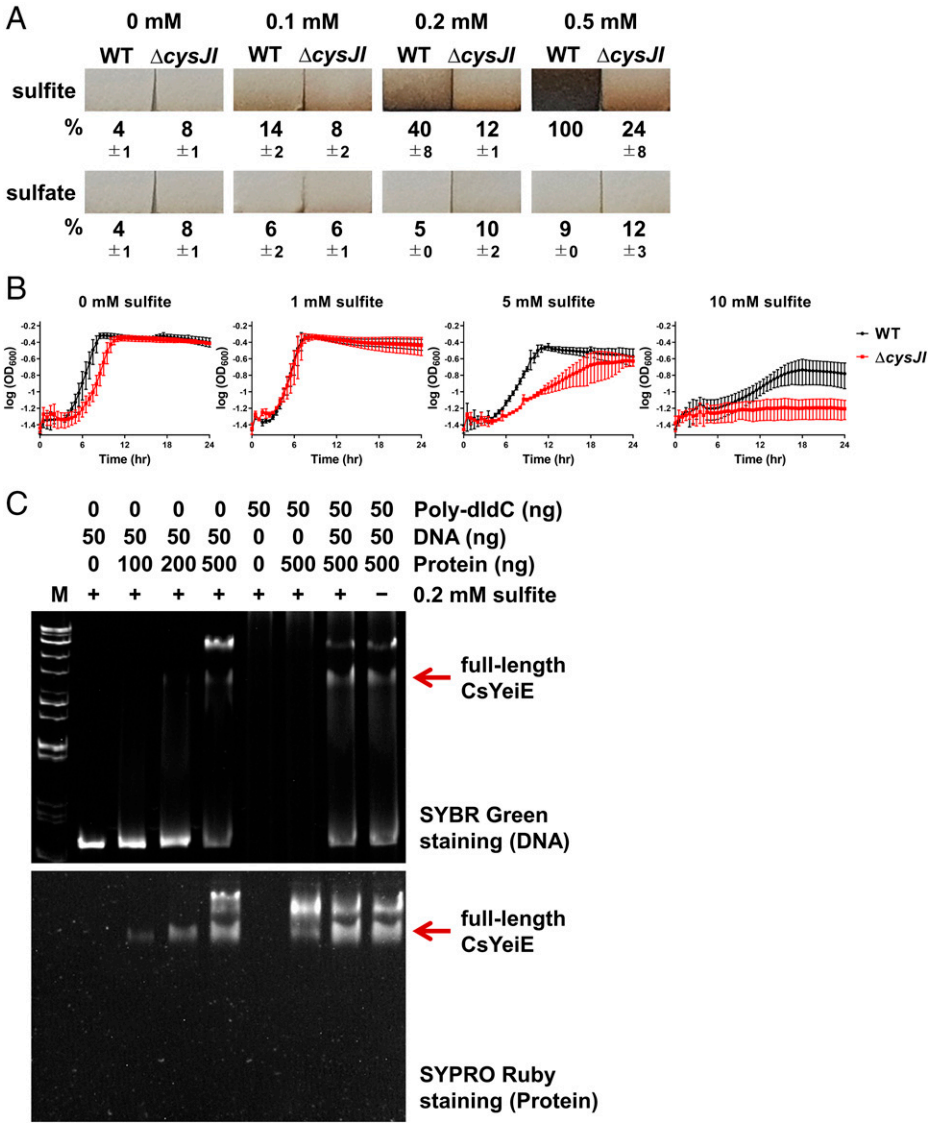

Fig. 5. Role of sulfite reductase CysJI in sulfite tolerance via YeiE. (*A*) The amount of H_2S production of the WT strain and Δ*cysJI* strain of *C. sakazakii* in liquid LB media was measured. The brown-stained paper strips show a result of the reaction with gaseous H_2S exiting in the liquid bacterial cultures. The percentages indicate the average level of H_2S production for each strain relative to the result of WT supplemented with 0.5 mM sulfite. The plus-minus sign represents SD values from three replicate experiments. (*B*) Growth curves of the WT strain and Δ*cysJI* strain of *C. sakazakii* in M9 media with Na_2SO_3 were measured by OD_{600}. The mean and SD values were calculated from three replicate experiments. The 0.5 mM cysteine was supplemented in the M9 media since CysJI is essential in cysteine biosynthesis. (*C*) EMSA with the purified FL CsYeiE protein was employed based on the promoter region of the *cysJI* gene. The poly(2′-deoxyinosinic-2′-deoxycytidylic acid) (poly-dIdC) was used to reduce nonspecific binding between DNA and the protein. The *Upper* panel represents the SYBR Green–stained gel for DNA, and the *Lower* panel represents the SYPRO Ruby–stained gel for protein. The red arrows on the *Right* represent the FL CsYeiE protein.

by far less impairment of sulfite resistance than the deletion of *yeiE* in the same culture condition (*SI Appendix*, Fig. S8*C*, over 0.5 mM). This difference implies that YeiE has other unknown mechanisms for sulfite resistance, in addition to the CysJI induction, to remove sulfite.

What would be the unknown mechanism of YeiE for bacterial resistance to sulfite? We noted catalase genes, because the Δ*yeiE* strain of *C. sakazakii* showed decreased viability when H_2O_2 was treated according to the previous report (25). In addition, it was known that the toxic sulfur trioxide anion radicals ($^{\bullet}SO_3^-$) and hydroxyl radicals ($^{\bullet}OH$) are produced via a nonenzymatic reaction in the coexistence of sulfite and H_2O_2 (43). We further observed that YeiE induced the *katG* gene, which is involved in ROS scavenging, in response to sulfite (*SI Appendix*, Fig. S11). Thus, the higher *katG* expression would account for the additional mechanism of YeiE for a bacterial survival strategy under high concentrations of sulfite. It would be important to investigate the additional mechanisms of YeiE in understanding the bacterial defense strategy against sulfite stress.

The LTTR CysL, commonly found in gram-positive bacteria, induced sulfite reductase in response to sulfate or sulfite in the media. Our findings, based on Glu145 in the structure of CsYeiE, suggested that only sulfite is the ligand for CysL, not sulfate (Fig. 2 and *SI Appendix*, Fig. S7). It is interesting that the *cysL*-deleted strain of *Bacillus subtilis* could not grow in both sulfate- and sulfite-containing media (35). Sulfate is metabolized to sulfite by multiple sequential enzymes (ATP sulfurylase, adenosine 5'-phosphosulfate (APS) kinase, and 3'-phosphoadenosine 5'-phosphosulfate (PAPS) reductase), regardless of CysL. Thus, sulfite would be accumulated and toxic to the bacteria in *cysL*-deleted bacteria due to the absence of sulfite reductase. These findings account for why the *cysL*-deleted strain of *B. subtilis* could not grow in the presence of sulfate.

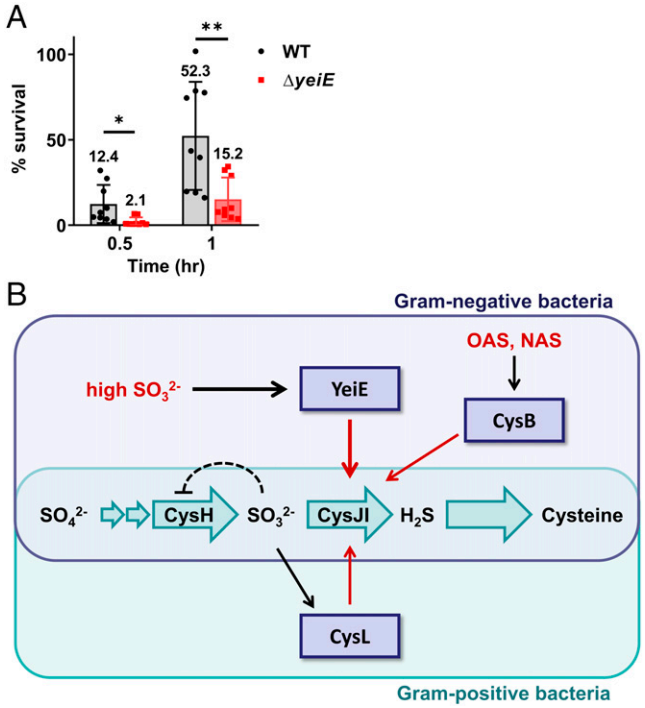

Fig. 6. Role of YeiE in the virulence of gram-negative bacteria. (*A*) Neutrophil extracellular killing assay performed to observe the survival percentages of the WT strain and Δ*yeiE* strain of *C. sakazakii* after incubation with freshly isolated neutrophils. The survival percentages of each strain were normalized toward the numbers of initial viable bacterial cells without treatment of neutrophils and visualized in columns, with a mean value above each column and error bar (n = 9). The P value was calculated with an unpaired t test using GraphPad Prism 8.0 software. *P < 0.05; **P < 0.005. (*B*) Schematic diagram of the roles of the LTTRs (violet boxes) YeiE, CysB, and CysL. In gram-negative bacteria, the LTTR CysB induces the basal expression of the sulfite reductase CysJI complex when *O*-acetylserine (OAS) and *N*-acetylserine (NAS) are accumulated in the cell. When gram-negative bacteria encounter a toxic concentration of sulfite (SO_3^{2-}), the LTTR YeiE directly activates the expression of CysJI. Gram-positive bacteria employ only one LTTR, CysL, to activate the expression of the CysJI complex in the presence of sulfite endogenously produced from sulfate (SO_4^{2-}). Sulfite produced by CysH remains low by an elaborate feedback mechanism. CysH, PAPS reductase; CysJI, sulfite reductase complex.

In gram-negative bacteria, the Δ*yeiE* strain of *C. sakazakii* could grow in the presence of sulfate, unlike the *cysL*-deleted strain of *B. subtilis* (*SI Appendix*, Fig. S8*D*). This observation shows different roles of the two LTTRs, CysB and YeiE, in gram-negative bacteria, compared to CysL in gram-positive bacteria. CysB is a master regulator of sulfate metabolism and cysteine biosynthesis and is regulated by the metabolic intermediates (44, 45). CysB transcriptionally activated *cysJI* like YeiE, although CysB is not regulated by sulfite. Further study is required to elucidate whether CysB and YeiE work together or independently regulate the *cysJI* transcriptional level. In contrast, gram-positive bacteria employ the LTTR CysL to sense the endogenous level of sulfite, thereby inducing the CysJI complex to metabolize sulfite in the cysteine biosynthesis pathway (Fig. 6*B*).

This study revealed a general resistance mechanism against sulfite, which is produced by fungi and host immune systems to combat bacteria. Since YeiE is commonly found in pathogenic gram-negative bacteria, inhibiting YeiE action may be a good target for restraining pathogenic bacteria. Furthermore, our findings also help broaden our knowledge of the appropriate use of sulfite by humans.

Materials and Methods

Protein Expression and Purification. The *yeiE* FL and RD gene from *C. sakazakii* ATCC 29544 (American Type Culture Collection) were inserted into the pET21d vector with the hexahistidine tag at the C terminus (EMD Biosciences) and the pProEx-HTa vector with the hexahistidine tag and tobacco etch virus (TEV) cleavage site at the N terminus (Thermo Fisher Scientific). The expression vector for the CsYeiE RD E145S mutant was constructed by site-directed mutagenesis with TOPsimple DyeMIX-nTaq PCR premix (Enzynomics) and Dpn1 restriction enzyme (TaKaRa) using the WT expression vector as the template. The plasmids were transformed into the *E. coli* BL21 (DE3) strain. The transformed cells were cultured in LB medium containing 100 μg/mL ampicillin at 37 °C until an optical density at 600 nm (OD_{600}) of 1.0 was measured. Then, the expression of proteins was induced by 0.5 mM isopropyl β-D-1-thiogalactopyranoside at 30 °C for 6 h. The cells harboring CsYeiE FL protein-expressing plasmids were resuspended in lysis buffer containing 20 mM Tris·HCl (pH 8.0), 150 mM NaCl, 5% (vol/vol) glycerol, and 5 mM 2-mercaptoethanol. The cells for the expression of CsYeiE RD proteins were lysed in buffer containing 50 mM Tris·HCl (pH 8.0), 150 mM NaCl, and 5 mM 2-mercaptoethanol. For CsYeiE RD E145S proteins, 20 mM Tris·HCl (pH 8.0) buffer containing 150 mM Na_2SO_4, 5% (vol/vol) glycerol, and 5 mM 2-mercaptoethanol was used for cell resuspension. The French press disrupted the resuspended cells, and the cell debris was subsequently removed by centrifugation at 19,000 × *g* for 30 min at 4 °C. The cell lysate was loaded onto nickel-nitrilotriacetic acid affinity agarose resin (GE Healthcare), and the target protein was eluted with lysis buffer supplemented with 250 mM imidazole. Eluted proteins were treated with TEV protease to remove the hexahistidine tag and further purified by anion exchange chromatography using a HiTrap Q column (GE Healthcare) with a linear increasing gradient of NaCl. The fractions were collected and loaded on a Superdex 200 HiLoad 26/600 column (GE Healthcare) in 20 mM Tris·HCl (pH 8.0) buffer containing 150 mM NaCl and 5 mM β-mercaptoethanol for size exclusion chromatography. For the CsYeiE RD E145S proteins, 10 mM Na_2SO_4 was supplemented in the size exclusion chromatography buffer.

Crystallization and Data Collection. The purified sulfite-bound CsYeiE RD, ligand-free CsYeiE RD, and sulfate-bound CsYeiE RD E145S were crystallized by the hanging-drop vapor diffusion method at 14 °C after mixing equal volumes (1 μL) of the protein and reservoir solution. A single crystal of sulfite-bound CsYeiE RD was obtained in a precipitation solution consisting of 0.1 M 2-(*N*-morpholino)ethanesulfonic acid (pH 7.0), 6% (vol/vol) polyethylene glycol (PEG) 20,000, and 2 mM Tris (2-carboxyethyl) phosphine. A single crystal of ligand-free CsYeiE RD was crystallized in a solution containing 0.1 M HEPES (pH 7.5), 11% (vol/vol) PEG 10,000, 6% (vol/vol) 2-methyl-2,4-pentanediol (MPD), and 50 μM Na_2SeO_3. A single crystal of sulfate-bound CsYeiE RD E145S was formed in a solution including 0.1 M HEPES (pH 7.5), 0.2 M $MgCl_2$, and 19% (vol/vol) PEG 3,350. The crystals of sulfite-bound CsYeiE RD, ligand-free CsYeiE RD, and sulfate-bound CsYeiE RD E145S were cryoprotected in a precipitant solution supplemented with 20% (vol/vol) glycerol, 30% (vol/vol) glycerol, and 20% (vol/vol) MPD, respectively, and flash-cooled in a liquid nitrogen stream at −173 °C. X-ray diffraction datasets were collected on the Beamline 5C at the Pohang Accelerator Laboratory (PAL).

Structural Determination and Refinement. X-ray diffraction data were processed using HKL2000 software (46). The structure of sulfite-bound CsYeiE RD was determined by the molecular replacement method with MOLREP (47) in the CCP4 package (48) using the model structure generated using the T-fold service, which is a part of the artificial intelligence–powered drug discovery platform (iDrug) by Tencent AI Lab (https://drug.ai.tencent.com/). The structures of ligand-free CsYeiE RD and sulfate-bound CsYeiE RD E145S were determined by the same molecular replacement method using the structure of sulfite-bound CsYeiE RD as the model structure. The final structures of CsYeiE RD were refined using the PHENIX software suite (49) (*SI Appendix*, Table S1).

ITC. ITC experiments were conducted using a MicroCal Auto-iTC200 (Malvern Panalytical) at the Korea Basic Science Institute. All samples were prepared in a buffer containing 20 mM Tris·HCl (pH 8.0) and 150 mM NaCl. The ligands (Na_2SO_3, sodium nitrate, and Na_2SO_4) used in the titration were purchased from Sigma-Aldrich. CsYeiE RD (32 μM) was prepared in the sample cell, and each

ligand (300 μM) was loaded into the syringe. The titrations were measured with 19 injections (2 μL) with 150-s spacing at 25 °C.

Bacterial Strains and Growth Assay. This study used the Δ*yeiE* strain of *C. sakazakii*, previously constructed (25). For the complementation study, the *yeiE* open reading frame was cloned in the pBAD18 plasmid, and the plasmid was transformed into Δ*yeiE* by electroporation. The Δ*cysJI* strain of *C. sakazakii* was constructed by the λ red recombination system (50). The *yeiE* deletion mutant of *E. coli* (*E. coli* Δ*yeiE*) and *E. coli* Δ*yeiE*+pYeiE were constructed following the same method used to construct the *C. sakazakii* strains. The *C. sakazakii* and *E. coli* strains and the plasmid used in this study are listed in *SI Appendix*, Table S2, and the primer sets are listed in *SI Appendix*, Table S3.

For the growth assay in M9 minimal media, the *C. sakazakii* and *E. coli* strains were precultured in a 14-mL round-bottom tube containing the intact M9 media (3 mL) at 37 °C overnight. The precultured cells were washed with a sulfate-deficient M9 media, prepared by substituting $MgSO_4$ with $MgCl_2$. Then, the cells were inoculated (at a 1:100 ratio) in a 24-well plate containing the sulfate-deficient M9 media (1 mL) and incubated with various concentrations of Na_2SO_3 or Na_2SO_4 at 37 °C. For the growth assay in LB media, the *C. sakazakii* strains were routinely cultured in LB media at 37 °C. The M9 and LB media were supplemented with 50 μg/mL ampicillin and 1.33 mM arabinose. For the Δ*cysJI* and Δ*yeiE* strains of *C. sakazakii* in Fig. 5*B* and *SI Appendix*, Fig. S8*C*, the *C. sakazakii* strains were precultured and main cultured in M9 media containing 0.5 mM cysteine. OD_{600} of the culture was measured, and the colony-forming unit (CFU) levels at each point were assessed by incubating diluted samples on the surface of LB agar plates for 12 h.

Measurement of H_2S Production. Gaseous H_2S production was measured using the $Pb(Ac)_2$ detection method (42). Paper strips saturated with 2% $Pb(Ac)_2$ were affixed to the inner wall of a culture tube above the level of the liquid culture of *C. sakazakii* or *E. coli* strains. Overnight cultures of the *C. sakazakii* or *E. coli* strains were diluted 1:50 in LB media with various Na_2SO_3 or Na_2SO_4 concentrations and incubated at 37 °C for 18 h at 200 rpm. Stained paper strips were quantified with ImageJ 1.53e (Wayne Rasband), and the results were normalized per the OD_{600} value.

RNA Extraction and Quantitative Real-Time PCR. The *C. sakazakii* strains were cultured in LB media with or without 0.2 mM Na_2SO_3 for 3 h at 37 °C. Total RNA was extracted from the cells at the exponential growth phase using an RNeasy Mini Kit (Qiagen) and synthesized into cDNA using EcoDry Premix and random hexamers (Takara). The synthesized cDNA was mixed with 2xiQ SYBR Green Supermix (Bio-Rad), and real-time PCR was performed. The primer sets are listed in *SI Appendix*, Table S3.

EMSA. The DNA fragment upstream of the *cysJI* genes was amplified using the primer sets described in *SI Appendix*, Table S3. EMSA was performed using an EMSA Kit (E33075; Invitrogen) according to the manufacturer's instructions. Briefly, the DNA-protein complex samples were run on 7% nondenaturing polyacrylamide gels at 200 V for 1 h. The DNA was stained by SYBR Green EMSA stain, and the protein was stained by SYPRO Ruby EMSA stain. The polyacrylamide gel was photographed by using a Geldoc instrument (Bio-Rad).

Neutrophil Extracellular Killing Assay. Bovine blood was collected at the local slaughterhouse (Anyang, Republic of Korea), and 1.5 mM ethylenediaminetetraacetic acid was added immediately to inhibit the coagulation of the blood. Neutrophils in whole blood were isolated based on the density gradient separation method (51). Briefly, Histopaque 1077 and Histopaque 1119 were used to generate a density gradient, and sequential centrifugation was performed to isolate neutrophils in a leukocyte suspension. The viability of the isolated neutrophils was confirmed by 0.4% (wt/vol) trypan blue staining. Neutrophils were seeded into 24-well plates at 2×10^5 cells/well. Cytochalasin D was added to 5 μg/mL to inhibit the phagocytic uptake of neutrophils for at least 30 min before bacterial infection. *C. sakazakii* strains were prepared by transferring a 1% (vol/vol) inoculum from an overnight culture into fresh LB broth and incubating for 3 h at 37 °C. The bacterial suspension was added to neutrophils at a multiplicity of infection of 1. The plate was centrifuged for 10 min at 500 × *g* and incubated at 37 °C with 5% CO_2. After incubation for two time points (0.5 and 1 h), the neutrophils were lysed with 0.02% (vol/vol) Triton X-100 for 10 min. Then, cultures were serially diluted, plated on LB agar, and incubated overnight to enumerate the CFU.

Data Availability. Structure data have been deposited in the Protein Data Bank (http://www.wwpdb.org/) (accession nos. 7ERP, 7ERQ, and 7FDF).

ACKNOWLEDGMENTS. We thank PAL (Pohang, Republic of Korea) for its Beamline 5C equipment and the ITC facility at the Korea Basic Science Institute (Ochang, Republic of Korea). This research was supported by the Bio & Medical Technology Development Program of the National Research Foundation (NRF), which is funded by the Ministry of Science & ICT (2019M3E5D6063871 to N.-C.H.). In addition, this research was also supported by the NRF funded by the Ministry of Education (2017H1A2A1042661: Global Ph.D. Fellowship Program to S.H.).

Author affiliations: [a]Department of Agricultural Biotechnology, Department of Food and Animal Biotechnology, Seoul National University, Seoul 08826, Republic of Korea; [b]Center for Food and Bioconvergence, Research Institute of Agriculture and Life Sciences, Seoul National University, Seoul 08826, Republic of Korea; and [c]Department of Pharmacy, College of Pharmacy and Institute of Pharmaceutical Sciences, CHA University, Gyeonggi-do 13488, Republic of Korea

1. B. Bar-Oz, A. Preminger, O. Peleg, C. Block, I. Arad, *Enterobacter sakazakii* infection in the newborn. *Acta Paediatr.* **90**, 356–358 (2001).
2. J. B. Gurtler, J. L. Kornacki, L. R. Beuchat, *Enterobacter sakazakii*: A coliform of increased concern to infant health. *Int. J. Food Microbiol.* **104**, 1–34 (2005).
3. N. R. Mullane *et al.*, *Enterobacter sakazakii* an emerging bacterial pathogen with implications for infant health. *Minerva Pediatr.* **59**, 137–148 (2007).
4. K. K. Lai, *Enterobacter sakazakii* infections among neonates, infants, children, and adults. Case reports and a review of the literature. *Medicine (Baltimore)* **80**, 113–122 (2001).
5. S. J. Forsythe, *Enterobacter sakazakii* and other bacteria in powdered infant milk formula. *Matern. Child Nutr.* **1**, 44–50 (2005).
6. A. B. Bowen, C. R. Braden, Invasive *Enterobacter sakazakii* disease in infants. *Emerg. Infect. Dis.* **12**, 1185–1189 (2006).
7. M. Friedemann, Epidemiology of invasive neonatal *Cronobacter* (*Enterobacter sakazakii*) infections. *Eur. J. Clin. Microbiol. Infect. Dis.* **28**, 1297–1304 (2009).
8. G. I. Dancer, J. H. Mah, M. S. Rhee, I. G. Hwang, D. H. Kang, Resistance of *Enterobacter sakazakii* (*Cronobacter* spp.) to environmental stresses. *J. Appl. Microbiol.* **107**, 1606–1614 (2009).
9. I. Hartmann *et al.*, Genes involved in *Cronobacter sakazakii* biofilm formation. *Appl. Environ. Microbiol.* **76**, 2251–2261 (2010).
10. S. M. Townsend *et al.*, *Enterobacter sakazakii* invades brain capillary endothelial cells, persists in human macrophages influencing cytokine secretion and induces severe brain pathology in the neonatal rat. *Microbiology (Reading)* **153**, 3538–3547 (2007).
11. C. N. Emami, R. Mittal, L. Wang, H. R. Ford, N. V. Prasadarao, Role of neutrophils and macrophages in the pathogenesis of necrotizing enterocolitis caused by *Cronobacter sakazakii*. *J. Surg. Res.* **172**, 18–28 (2012).
12. A. Baumgartner, M. Grand, M. Liniger, C. Iversen, Detection and frequency of *Cronobacter* spp. (*Enterobacter sakazakii*) in different categories of ready-to-eat foods other than infant formula. *Int. J. Food Microbiol.* **136**, 189–192 (2009).
13. J. Chap *et al.*, International survey of *Cronobacter sakazakii* and other *Cronobacter* spp. in follow up formulas and infant foods. *Int. J. Food Microbiol.* **136**, 185–188 (2009).
14. B. Healy *et al.*, *Cronobacter* (*Enterobacter sakazakii*): An opportunistic foodborne pathogen. *Foodborne Pathog. Dis.* **7**, 339–350 (2010).
15. M. C. Kandhai, M. W. Reij, L. G. Gorris, O. Guillaume-Gentil, M. van Schothorst, Occurrence of *Enterobacter sakazakii* in food production environments and households. *Lancet* **363**, 39–40 (2004).
16. K. Kim *et al.*, Prevalence and genetic diversity of *Enterobacter sakazakii* in ingredients of infant foods. *Int. J. Food Microbiol.* **122**, 196–203 (2008).
17. M. F. Christman, G. Storz, B. N. Ames, OxyR, a positive regulator of hydrogen peroxide-inducible genes in *Escherichia coli* and *Salmonella typhimurium*, is homologous to a family of bacterial regulatory proteins. *Proc. Natl. Acad. Sci. U.S.A.* **86**, 3484–3488 (1989).
18. C. Michán, M. Manchado, G. Dorado, C. Pueyo, *In vivo* transcription of the *Escherichia coli oxyR* regulon as a function of growth phase and in response to oxidative stress. *J. Bacteriol.* **181**, 2759–2764 (1999).
19. K. M. Gebendorfer *et al.*, Identification of a hypochlorite-specific transcription factor from *Escherichia coli*. *J. Biol. Chem.* **287**, 6892–6903 (2012).
20. B. W. Parker, E. A. Schwessinger, U. Jakob, M. J. Gray, The RclR protein is a reactive chlorine-specific transcription factor in *Escherichia coli*. *J. Biol. Chem.* **288**, 32574–32584 (2013).
21. I. Jo *et al.*, Structural details of the OxyR peroxide-sensing mechanism. *Proc. Natl. Acad. Sci. U.S.A.* **112**, 6443–6448 (2015).
22. S. E. Maddocks, P. C. F. Oyston, Structure and function of the LysR-type transcriptional regulator (LTTR) family proteins. *Microbiology (Reading)* **154**, 3609–3623 (2008).
23. I. Jo *et al.*, Structural basis for HOCl recognition and regulation mechanisms of HypT, a hypochlorite-specific transcriptional regulator. *Proc. Natl. Acad. Sci. U.S.A.* **116**, 3740–3745 (2019).
24. Y. Jang *et al.*, A novel tetrameric assembly configuration in VV2_1132, a LysR-type transcriptional regulator in *Vibrio vulnificus*. *Mol. Cells* **41**, 301–310 (2018).
25. Y. Choi *et al.*, Possible roles of LysR-type transcriptional regulator (LTTR) homolog as a global regulator in *Cronobacter sakazakii* ATCC 29544. *Int. J. Med. Microbiol.* **302**, 270–275 (2012).
26. Y. Gao *et al.*, Systematic discovery of uncharacterized transcription factors in *Escherichia coli* K-12 MG1655. *Nucleic Acids Res.* **46**, 10682–10696 (2018).

27. T. Fujii, Y. Aritoku, H. Agematu, H. Tsunekawa, Increase in the rate of L-pipecolic acid production using lat-expressing *Escherichia coli* by *lysP* and *yeiE* amplification. *Biosci. Biotechnol. Biochem.* **66**, 1981–1984 (2002).
28. T. L. Westerman, M. K. Sheats, J. R. Elfenbein, Sulfate import in *Salmonella* Typhimurium impacts bacterial aggregation and the respiratory burst in human neutrophils. *Infect. Immun.* **89**, e00701-20 (2021).
29. T. L. Westerman, M. McClelland, J. R. Elfenbein, YeiE regulates motility and gut colonization in *Salmonella enterica* serotype Typhimurium. *mBio* **12**, e0368020 (2021).
30. I. Jo *et al.*, The hydrogen peroxide hypersensitivity of OxyR2 in *Vibrio vulnificus* depends on conformational constraints. *J. Biol. Chem.* **292**, 7223–7232 (2017).
31. H. Choi *et al.*, Structural basis of the redox switch in the OxyR transcription factor. *Cell* **105**, 103–113 (2001).
32. D. M. Mahounga, H. Sun, Y. L. Jiang, Crystal structure of the effector-binding domain of *Synechococcus elongatus* CmpR in complex with ribulose 1,5-bisphosphate. *Acta Crystallogr. F Struct. Biol. Commun.* **74**, 506–511 (2018).
33. J. L. Taylor *et al.*, The crystal structure of AphB, a virulence gene activator from *Vibrio cholerae*, reveals residues that influence its response to oxygen and pH. *Mol. Microbiol.* **83**, 457–470 (2012).
34. S. M. Prezioso, K. Xue, N. Leung, S. D. Gray-Owen, D. Christendat, Shikimate induced transcriptional activation of protocatechuate biosynthesis genes by QuiR, a LysR-type transcriptional regulator, in *Listeria monocytogenes*. *J. Mol. Biol.* **430**, 1265–1283 (2018).
35. I. Guillouard *et al.*, Identification of *Bacillus subtilis* CysL, a regulator of the *cysJI* operon, which encodes sulfite reductase. *J. Bacteriol.* **184**, 4681–4689 (2002).
36. A. Mironov *et al.*, Mechanism of H_2S-mediated protection against oxidative stress in *Escherichia coli*. *Proc. Natl. Acad. Sci. U.S.A.* **114**, 6022–6027 (2017).
37. K. Shatalin *et al.*, Inhibitors of bacterial H_2S biogenesis targeting antibiotic resistance and tolerance. *Science* **372**, 1169–1175 (2021).
38. H. Mitsuhashi *et al.*, Sulfite is released by human neutrophils in response to stimulation with lipopolysaccharide. *J. Leukoc. Biol.* **64**, 595–599 (1998).
39. P. Frey-Klett *et al.*, Bacterial-fungal interactions: Hyphens between agricultural, clinical, environmental, and food microbiologists. *Microbiol. Mol. Biol. Rev.* **75**, 583–609 (2011).
40. W. Dott, Sulfite formation by wine yeasts. I. Relationships between growth, fermentation and sulfite formation. *Arch. Microbiol.* **107**, 289–292 (1976).
41. A. R. Garcia-Fuentes, S. Wirtz, E. Vos, H. Verhagen, Short review of sulphites as food additives. *Eur. J. Nutr. Food Saf.* **5**, 113–120 (2015).
42. K. Shatalin, E. Shatalina, A. Mironov, E. Nudler, H_2S: A universal defense against antibiotics in bacteria. *Science* **334**, 986–990 (2011).
43. C. Mottley, T. B. Trice, R. P. Mason, Direct detection of the sulfur trioxide radical anion during the horseradish peroxidase-hydrogen peroxide oxidation of sulfite (aqueous sulfur dioxide). *Mol. Pharmacol.* **22**, 732–737 (1982).
44. M. Mittal, A. K. Singh, S. Kumaran, Structural and biochemical characterization of ligand recognition by CysB, the master regulator of sulfate metabolism. *Biochimie* **142**, 112–124 (2017).
45. E. Guédon, I. Martin-Verstraete, "Cysteine metabolism and its regulation in bacteria" in *Amino Acid Biosynthesis– Pathways, Regulation and Metabolic Engineering*, V. F. Wendisch, Ed. (Springer, Berlin, 2007), pp. 195–218.
46. Z. Otwinowski, W. Minor, Processing of X-ray diffraction data collected in oscillation mode. *Methods Enzymol.* **276**, 307–326 (1997).
47. A. Vagin, A. Teplyakov, Molecular replacement with MOLREP. *Acta Crystallogr. D Biol. Crystallogr.* **66**, 22–25 (2010).
48. M. D. Winn *et al.*, Overview of the CCP4 suite and current developments. *Acta Crystallogr. D Biol. Crystallogr.* **67**, 235–242 (2011).
49. P. D. Adams *et al.*, PHENIX: A comprehensive Python-based system for macromolecular structure solution. *Acta Crystallogr. D Biol. Crystallogr.* **66**, 213–221 (2010).
50. K. A. Datsenko, B. L. Wanner, One-step inactivation of chromosomal genes in *Escherichia coli* K-12 using PCR products. *Proc. Natl. Acad. Sci. U.S.A.* **97**, 6640–6645 (2000).
51. D. W. Siemsen *et al.*, Neutrophil isolation from nonhuman species. *Methods Mol. Biol.* **1124**, 19–37 (2014).
52. R. A. Laskowski, M. B. Swindells, LigPlot+: Multiple ligand-protein interaction diagrams for drug discovery. *J. Chem. Inf. Model.* **51**, 2778–2786 (2011).